JTTEE5 15:790-795
DOI: 10.1361/105996306X146785
1059-9630/$19.00 © ASM International

Peer Reviewed

Optimization of Laser Cladding Process Using Taguchi and EM Methods for MMC Coating Production

L. Dubourg and L. St-Georges

(Submitted May 8, 2006; in revised form July 10, 2006)

This study investigates the influence of laser cladding parameters on the geometry and composition of metal-matrix composite (MMC) coatings. Composite coatings are made of a Ni-Cr-B-Si metallic matrix and of WC reinforcement with a volume fraction of 50%. Optical microscopy is used to characterize the coating geometry (height, width, and penetration depth) and to determine the real volumetric content of WC. Laser cladding on low-carbon steel substrate is carried out using a cw neodymium:yttrium-aluminum-garnet (Nd:YAG) laser, a coaxial powder injection system, and a combination of Taguchi and EM methods to design the experiments. This combination explores efficiently the multidimensional volume of laser cladding parameters. The results, which express the interrelationship between laser cladding parameters and the characteristics of the clad produced, can be used to find optimum laser parameters, to predict the responses, and to improve the understanding of laser cladding process.

Keywords influence of spray parameters, laser deposited materials, porosity of coatings

1. Introduction

As shown in Fig. 1, laser cladding consists of covering a substrate surface with a coating of a different nature. This process can be carried out in several ways: with wire feed, lateral (Ref 1), or coaxial (Ref 2) powder injection (Fig. 1). In the case of powder injection, the cladding powder is injected into the laser beam by an inert gas flow. The energy delivered by the laser is absorbed both by the powder stream and the substrate material. This enables the melting of the in-flight particles and the fusing of the powder onto the substrate surface. A clad is formed by moving the sample under the laser beam. A uniform layer is obtained by partially overlapping individual clads. A slight dilution of the cladding material into the substrate generates a perfect metallurgical bonding between them. Many studies on laser surface treatment have been carried out with the goal of improving the mechanical characteristics of clad coatings (hardness, elastic modulus, and wear resistance). These studies were done on steel (Ref 3, 4), aluminum (Ref 5-11), and magnesium (Ref 12) substrates. Several authors have already investigated the formation of intermetallic compounds such as Al_yX_z (alloys Al-Ni, Ref 5; Al-Si, Ref 6; Al-Cu, Ref 7; Al-Mo, Ref 8; and Al-Cr, Ref 9) for aluminum treatment and Mg_yX_z (alloys Mg-Al, Ref 12) for magnesium treatment. Another field of research consists of the development of metal-matrix composites (MMC) coatings. These materials are composed of hard reinforcement particles distributed in a softer metal matrix. In the case of steel, the most-used reinforcement particles are tungsten carbide (Ref 3, 4), due to their relative low cost and high mechanical properties. On the other hand, for aluminum and magnesium surface treatment, the reinforcements are more often silicon carbide (Ref 10) or titanium carbide (Ref 11) due to their low densities. Studies show that no significant difference of wear resistance is observed among laser clad MMC coatings containing TiC, SiC, or WC particles, although the mechanical characteristics of these different reinforcement particles are dissimilar (Ref 13). In the current study, coatings are made from a nickel-base matrix and WC with a volume fraction of 50%. The study investigates the influence of the laser cladding parameters on the geometry and composition of MMC coatings. Experiments are done on low-carbon steel substrates. The laser cladding is carried out using a coaxial powder injection system and a neodium:yttrium-aluminum-garnet (Nd:YAG) laser. An optical microscope is used to analyze and characterize the coating geometry.

2. Experimental Setup

Laser cladding is performed with a continuous wave 4000 W Nd:YAG laser of 1064 mm wavelength and a 600 μm diameter optical fiber. A lens with a 280 mm focal length is used to focus the laser beam. The laser beam power is adjusted to 4000 W on the workpiece surface and defocused with an out-of-focus distance from 45 to 70 mm. For this out-of-focus distance range, the spot diameter on the workpiece evolves from 6 to 8 mm (see Fig. 2). Accordingly, the power density varies from 141 to 80 W/mm^2. At the same time, the power distribution of the laser beam also evolves from a flat top profile at the focus point to a Gaussian profile at a defocused position (as presented in Fig. 2). Cladding speed varies from 0.4 to 1.6 m/min. The substrates are

This article was originally published in *Building on 100 Years of Success, Proceedings of the 2006 International Thermal Spray Conference* (Seattle, WA), May 15-18, 2006, B.R. Marple, M.M. Hyland, Y.-Ch. Lau, R.S. Lima, and J. Voyer, Ed., ASM International, Materials Park, OH, 2006.

L. Dubourg, Aerospace Manufacturing Technology Centre, National Research Council Canada, Montreal and REMAC Industrial Innovators Inc., Saguenay, Quebec, Canada; and **L. St-Georges,** REMAC Industrial Innovators Inc., Saguenay, Quebec, Canada. Contact e-mail: Laurent.dubourg@cnrc-nrc.gc.ca.

composed of Fe-0.06 C (wt.%) and the sample size is 50 × 50 × 12 mm^3. The powders of prealloyed nickel-base matrix (Ni-4B-5Si-5Fe-10Cr, wt.%) and reinforcement particles are premixed prior to the injection with a volume fraction of 50%. The resulting mixture is injected inside the laser beam at a rate ranging from 30 to 120 g/min.

In the investigation presented here, the influence of the laser cladding parameters (cladding speed, powder feed rate, out-of-focus distance, and overlapping) on coating geometry is studied. A combination of Taguchi and experimentation and modelization (EM) design of experiments is used to optimize the cladding parameters and minimize the number of tests and characterizations. The Taguchi method relies on a normalized orthogonal matrix. Each set of matrices ensures that the space is investigated in a way that the effect of every variable can be clearly detected. This can be done by varying many parameters at the same time along the orthogonal border of the orthogonal domain. For example, Fig. 3(a) shows an L9 matrix for two factors with three levels. Alternatively, EM technique is based on the Euclidian domain elaboration, which is modified in an interactive way by varying all the parameters at the same time. The process feasibility domain is then defined by a multidimensional volume that discriminates the accepted tests inside this volume and the rejected tests outside it. Figure 3(b) illustrates this feasibility domain (blue zone). This method allows a more interactive approach using a dynamic construction of the feasibility domain throughout the data collection. In the current study, a combination of Taguchi and EM methods called Taguchi/EM is used as shown in Fig. 3(c). As the first step, the feasibility domain is promptly defined by an L18 Taguchi matrix and the multidimensional volume is efficiently explored (red square plots in Fig. 3c). Subsequently, the EM method is used to refine the domain (blue plots in Fig. 3c), to find the key indicators that can explain the response variations and to optimize the cladding process. In the case of laser welding, this hybrid Taguchi/EM method has previously provided equivalent prediction models with less experimental tests than the ones provided by classic methods (Ref 14, 15).

To characterize the coatings, the cross section of the coatings is polished to a mirror finish (diamond paste with a grain size of 1 μm). The coating geometry is evaluated using an optical microscope. Two tests are performed: a clad made in a single pass

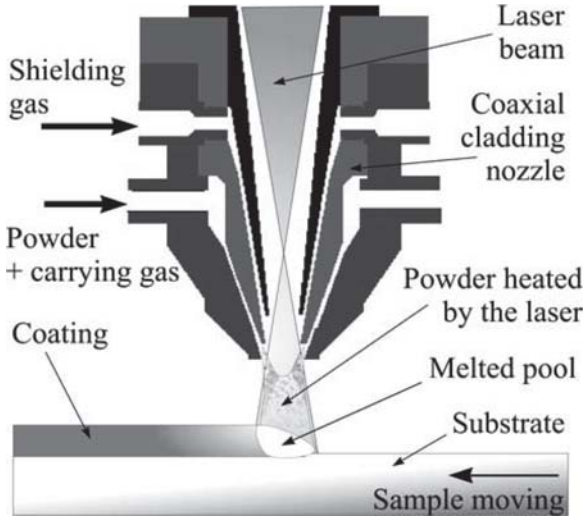

Fig. 1 Principle of laser cladding with coaxial powder injection

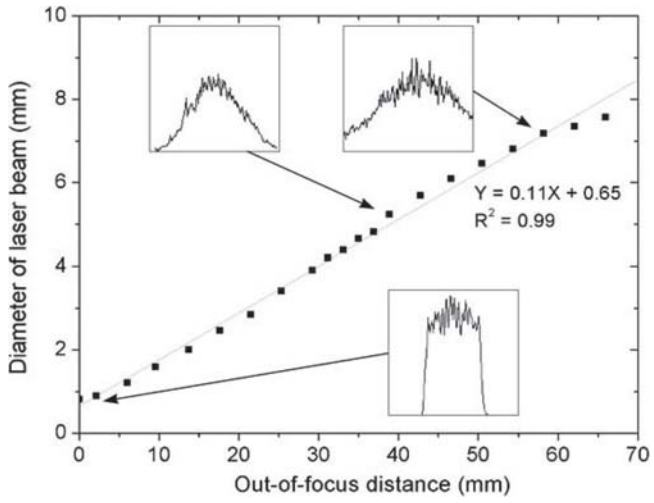

Fig. 2 Effect of the out-of-focus distance on the shape and the diameter of the laser beam

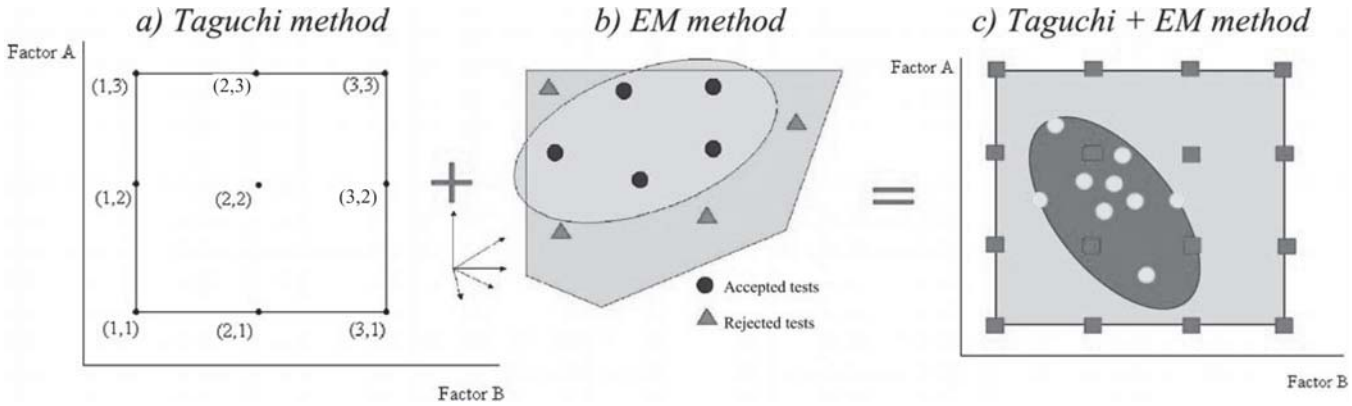

Fig. 3 (a) Example of Taguchi method: L9 design for two factors at three level each. (b) Example of EM method: feasibility domain of the process (blue zone). (c) Example of Taguchi/EM method (■, point obtained with Taguchi; ●, point obtained with EM; blue zone, feasibility domain; yellow zone, domain explored with the Taguchi method)

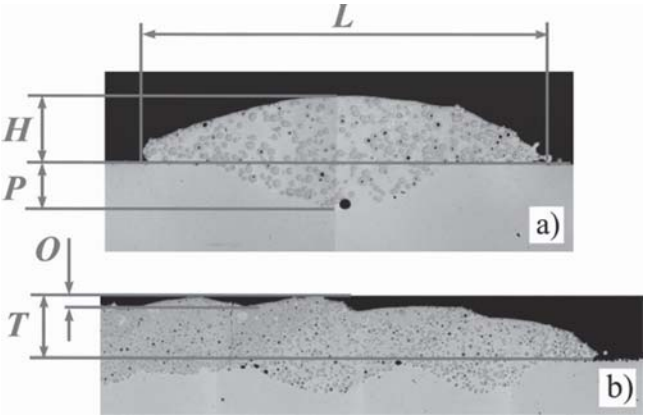

Fig. 4 Dimensions measured for clad characterization: (a) clad made in a single pass; (b) clad made in multiple passes, obtained by overlapping

(Fig. 4a) and a coating made in multiple passes, obtained by overlapping (Fig. 4b). The distance from the surface substrate to the deeper point in the substrate is defined as the penetration depth (P). On the overlapping coating, the coating thickness (T) and the overthickness (O) are measured as shown in Fig. 4(b). For the reinforcement particle measurements, optical microscopy images are digitalized and analyzed using image analysis software. The reinforcement particles are isolated, implementing several filtering protocols. Five images defined randomly across the cross section are analyzed on each sample, and the results are subsequently averaged.

3. Results and Discussion

With the Taguchi/EM method, two steps are considered. An L18 matrix is used in the first step, combining four input parameters with four levels each, for a total of 18 trials. These input parameters are the laser scanning (ranging from 400 to 1600 mm/min by step of 0.4 m/min), the powder feed rate (ranging from 30 to 120 g/min by step of 30 g/min), the out-of-focus distance (ranging from 50 to 65 mm by step of 5 mm), and the overlapping for multipass cladding (ranging from 4 to 7 mm by step of 1 mm). This exercise promptly defines the feasibility domain and explores efficiently the multidimensional volume. In the second step, the interactive EM technique is used, varying all the parameters at the same time. The domain is refined test after test, and each subsequent test is selected to maximize the gain in new information. This method takes a more interactive approach, leading to the dynamic construction of the feasibility domain throughout the data collection. After these two steps, the feasibility domain is well known, and the prediction equations are stable (Ref 14, 15). All regression equations modeling the different responses as function of the input parameters show R^2 regression coefficients above 70%, indicating a good fit.

3.1 Single-Pass Coating

For a single-pass coating, Fig. 5 shows the Pareto charts of the height (H) and the width (L) as a function of cladding parameters. The Pareto chart is an illustration of the estimated effects of the input parameters. The length of each bar on the chart is proportional to the positive or negative standardized effect.

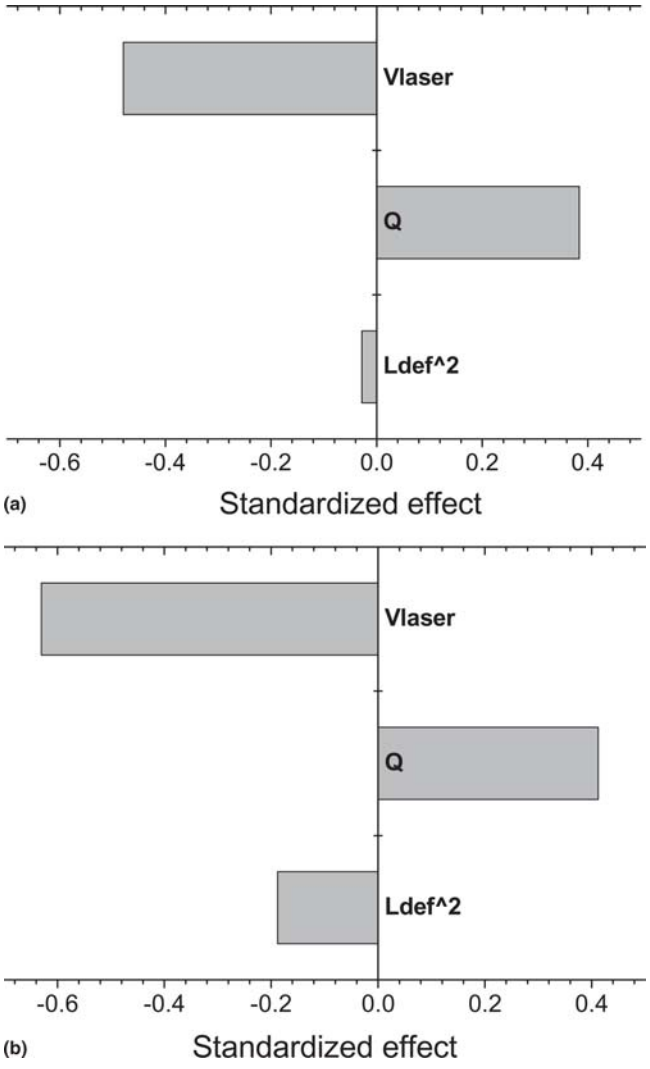

Fig. 5 Pareto charts of (a) the height (H) of single-pass clad and (b) the width (L) of single-pass clad. Input parameters: cladding speed (V_{laser}), powder feed rate (Q), and square of the out-of-focus distance (L_{def}^2).

According to Fig. 5, the clad size (i.e., height and width) is influenced by the cladding speed (V_{laser}, in mm/min) and the powder feed rate (Q, in g/min). As depicted in the Pareto chart, the influence of the cladding speed has a negative coefficient. When the cladding speed is lower, more powder is deposited on a given area of the substrate, and consequently, the clad size increases. In contrast, the powder feed rate has a direct effect on the clad size (as illustrated by the positive value in the Pareto chart). For an increased feed rate, more powder is added on the substrate and, similarly, the clad size increases. The effect of the out-of-focus distance is less pronounced than the two other parameters considered here. The out-of-focus distance has mainly an influence on the area of the laser beam spot and, consequently, on the laser power density. This does not considerably influence the clad size. As the out-of-focus distance increases, the laser power density decreases and fewer in-flight particles can be melted, as shown by the negative effect of the out-of-focus distance on the clad height and width. Nevertheless, for the range of out-of-focus distances considered here, the power den-

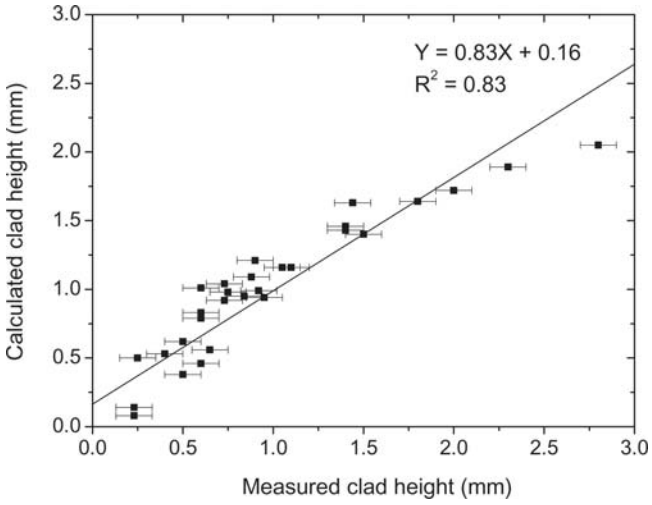

Fig. 6 Calculated clad height according to Eq 1 as function of the measured clad height

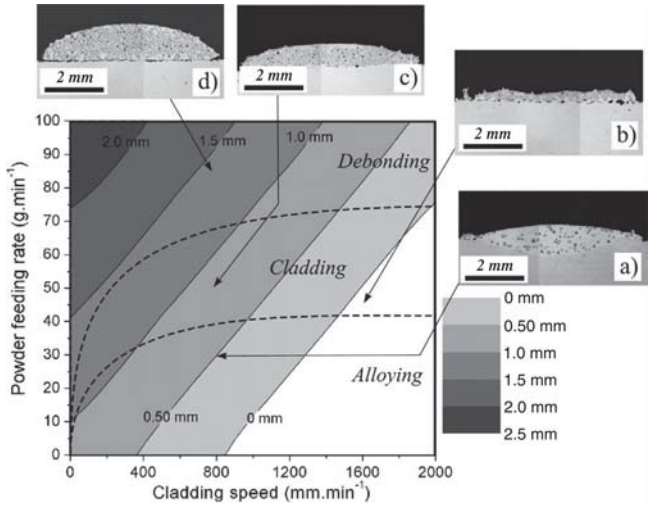

Fig. 7 Types of cladding obtained as a function of the cladding speed and powder feed rate. (a) Surface alloying, (b) cladding with roughness, pores, and cracks, (c) good cladding, and (d) debonding cladding

sity seems to be large enough to tolerate small variations of the power density and melt appropriately the injected powders. This phenomenon is a paradox as, at first sight, one may think that an increase of the laser beam spot leads to an increase of the clad width. According to the very small effect of the out-of-focus distance on the single-pass clad height, the height can be correctly predicted only by the cladding speed and the powder feed rate and expressed by:

$$H = 0.86 - 0.0011V_{laser} + 0.016Q \quad \text{(Eq 1)}$$

To validate this predictive model, the result of this equation is plotted as a function of the experimental data in Fig. 6. The good relationship between the two sets of results (r^2 equal to 0.83) confirms the negligible effect of the out-of-focus distance on the clad height and the validity of the predictive model developed here.

During this experiment, variations in the geometry and the quality of the cladding coating are observed. These variations are collected and used to produce the chart illustrated in Fig. 7. Three principal zones are then identified as a function of the cladding speed and the powder feed rate, for various clad thickness: the debonding zone, the cladding zone, and the alloying zone. In Fig. 7, these zones are separated by dotted lines. In the alloying and the cladding zone, the powder is fused onto the substrate surface, resulting in a good metallurgical bonding. In the debonding zone, a poor metallurgical bonding is obtained. Typically, four different geometries in the clad cross section are observed. These four geometries, illustrated in Fig. 7, can be described as:

- *Surface alloying (Fig. 7a):* In this zone, elevated cladding speeds are combined with low powder feed rates. The laser energy is mainly absorbed by the substrate and the dilution is important. The clad has a good bond with the substrate. However, the clad is a combination of cladding material and substrate; the WC content is then low.
- *Cladding with roughness, pores, and cracks (Fig. 7b):* This clad has a good bond with the substrate and a low dilution. However, its surface exhibits high roughness, porosity, and cracks.
- *Good cladding (Fig. 7c):* In this region, a good bond between the substrate and the clad is observed. The clad has a smooth surface and good profile without cracks and pores. A low dilution is obtained.
- *Debonding cladding (Fig. 7d):* No bonding is created due to the significant lack of laser energy on the workpiece (high powder feed rate and low cladding speed). The energy is sufficient to melt the in-flight particles only. The clad in this region is easily removed after the process.

In Fig. 7, the clad height is also represented as a function of the cladding speed and powder feed rate according to Eq 1. Various gray scales illustrate various clad thicknesses. According to the zones identified previously, this figure illustrates the limitation of the process in terms of clad height. For example, if a clad with a height exceeding 1.5 mm is obtained, debonding should be expected. A good clad has typically a maximum thickness of 1.5 mm.

The methodology described previously is also used to evaluate the effect of cladding parameters on the WC content of a single pass clad. The parameters are the cladding speed (V_{laser}), the powder feed rate (Q), and the out-of-focus distance (L_{def}). The Pareto chart obtained is presented in the Fig. 8. As depicted in this chart, the powder feed rate is the governing parameter, followed by the out-of-focus distance and the cladding speed. The effects of these parameters are drastically different than the ones observed for the clad size. Consequently, no direct relationship can be expressed between the size and the WC content of the clad. According to Fig. 7, the powder feed rate mainly governs the bonding quality between the clad and the substrate. As the powder feed rate increases, the amount of laser power absorbed by the in-flight particles increases and less dilution is observed. This reduction of dilution has a direct impact on the chemical clad composition and results in higher WC content. In fact, when the dilution becomes more important, the chemical clad composition becomes a combination of the cladding material and substrate (reduction of the WC content). As the cladding speed increases, the energy transmitted to a given area of the substrate decreases and less dilution is observed, resulting in a

higher WC concentration. The effect of the out-of-focus distance on the WC content is similar. This distance has a direct effect on the power density of the laser beam. As the out-of-focus distance increases, the area of the laser spot increases, and consequently for a constant laser power the power density is lowered. Less dilution is then obtained (higher WC content observed). Moreover, an increase of the laser spot can lead to a larger molten pool under the laser beam, increasing the quantity of powders going into it and the WC content. Nevertheless, this explanation disagrees with the previous observation made in Fig. 5(b): a higher laser spot does not lead to a higher clad width. This phenomenon cannot be taken into account. Using these parameters, the predicting equation of the WC content (in vol.%) as a function of the powder feed rate (Q) and the out-of-focus distance (L_{def}, in mm) is obtained:

$$WC(\%) = -18.95 + 0.33Q + 0.55L_{def} \quad \text{(Eq 2)}$$

In Fig. 9, the numerical prediction of the WC content obtained using Eq 2 is compared with the experimental measurements. Again, the predictions are in good agreement with the experiments ($r^2 = 0.74$). The interrelationship between the laser cladding parameters and the WC clad content can be correctly predicted.

3.2 Multipass Coating

The same methodology is used to analyze the effect of the cladding parameters on the coating thickness (T) of multipass cladding. The resulting Pareto chart is shown in Fig. 10. For the multipass cladding, similarly to the single-pass cladding, the coating thickness is mainly predicted by the cladding speed and the powder feed rate. Surprisingly, for the range of overlapping (n) used in this study, this parameter does not have a big impact on the coating thickness. To understand this behavior, the global geometry of the coating is analyzed. The overlapping does not have a direct effect on the thickness, but has a major impact on the global geometry of the coating, as presented below. Neglecting the effect of the out-of-focus distance and overlapping, the coating thickness can be expressed as Eq 3. This equation is close to Eq 1, except for the nominal term: 0.86 mm for single pass and 1.51 mm for multipass cladding. Using this equation, the coating thickness can be correctly predicted, as shown in Fig.

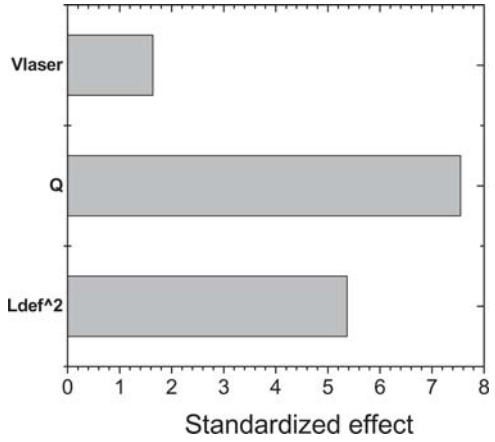

Fig. 8 Pareto chart of the WC content of single-pass clad. Input parameters: cladding speed (V_{laser}), powder feed rate (Q), and out-of-focus distance (L_{def})

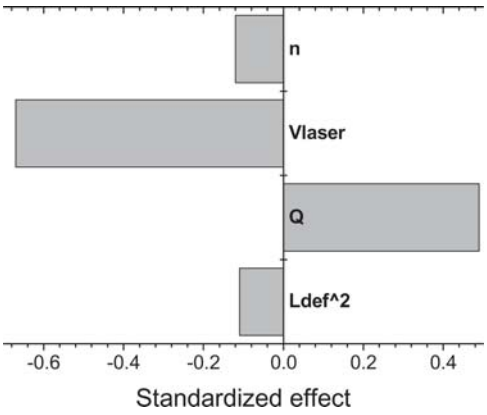

Fig. 10 Pareto charts of the thickness (T) of multipass cladding. Parameters: cladding speed (V_{laser}), powder feed rate (Q), square of out-of-focus distance (L_{def}^2) and overlapping (n)

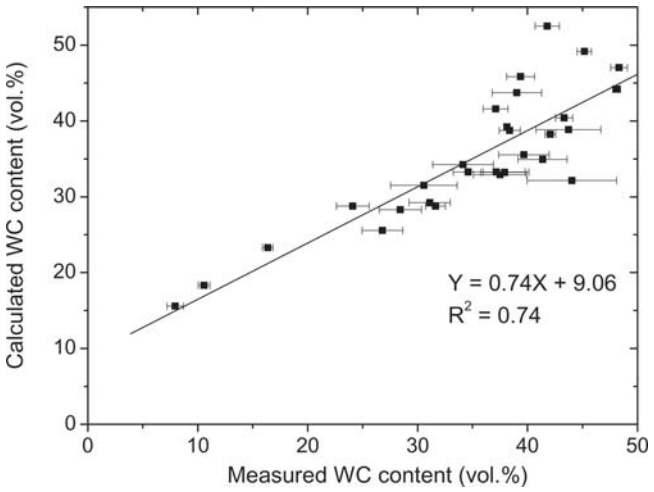

Fig. 9 Calculated WC content according to Eq 2 as a function of the measured WC content

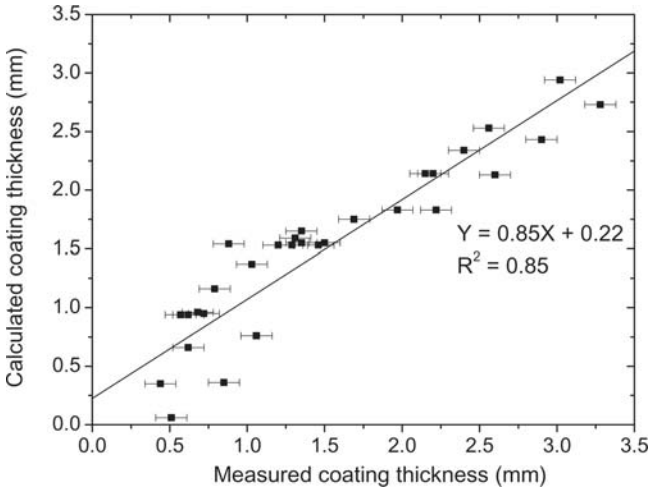

Fig. 11 Calculated coating thickness for multipass cladding according to Eq 3 as a function of the measured coating thickness

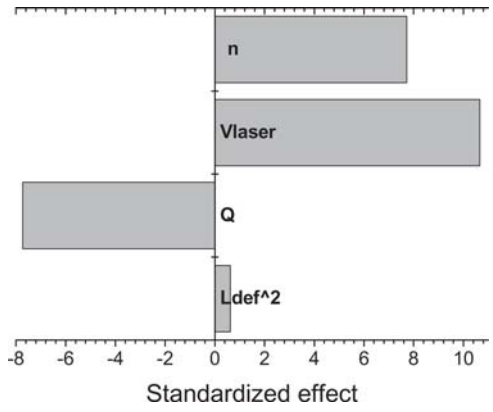

Fig. 12 Pareto charts of the relative overthickness of multipass cladding. Input parameters: cladding speed (V_{laser}), powder feed rate (Q), out-of-focus distance (L_{def}^2), and overlapping (n)

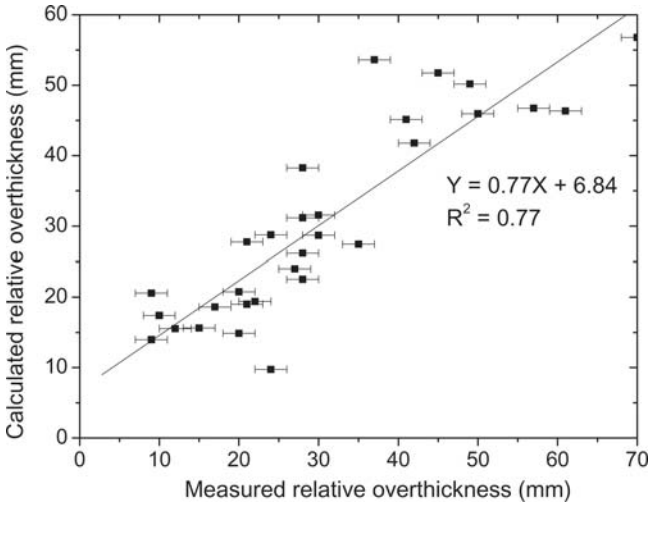

Fig. 13 Calculated relative overthickness for multipass cladding according to Eq 4 as a function of the measured relative overthickness

11. In this graph, a good correlation between the numerical predictions and the experimental results is observed.

$$T = 1.51 - 0.001V_{laser} + 0.020Q \quad \text{(Eq 3)}$$

For multipass cladding, the overthickness is also analyzed. This parameter is partially representative of the global coating geometry, as presented before in Fig. 4, and cannot be analyzed alone. Without any relationship with the total coating thickness, no correlation can be established between the overthickness and the cladding parameters. To determine the relative effect of cladding parameters on the global geometry of multipass cladding, it is required to define a new parameter, which considers the overthickness (O) relative to the global thickness of the coating (T). This new parameter, called the relative overthickness (RO), can be defined as $RO = O/T$. Using this new parameter, a good correlation can be established between the global geometry of multipass cladding and the cladding parameters. As illustrated in Fig. 12, the relative overthickness is governed by the cladding speed (V_{laser}), the overlapping (n, in mm), and the powder feed rate (Q). This relationship, written in a numerical form in Eq 4, can be visually validated by the Fig. 13, where the numerical predictions are compared with the experimental measurements.

$$RO = -12.49 + 0.023V_{laser} - 0.334Q + 8.460n \quad \text{(Eq 4)}$$

4. Conclusions

Using a combination of Taguchi and EM methods to design the experiments, the influence of different laser cladding parameters on the clad geometry and the WC content is investigated. For single-pass and multipass cladding, the predominant effects of the cladding speed and the powder feed rate on the clad size are confirmed. A relationship between the cladding parameters and the WC content is established, and the influence of the out-of-focus distance was observed. For the multipass cladding, a new parameter is defined to understand and predict the effect of the cladding parameters on the final geometry of a multipass cladding.

Acknowledgments

The authors thank Martin Larouche for laser cladding experiments and Hélène Grégoire and Dany Drolet for metallography and image analysis.

References

1. Y. Li, H. Yang, X. Lin, W. Huang, J. Li, and Y. Zhou, The Influences of Processing Parameters on Forming Characterizations During Laser Rapid Forming, *Mater. Sci. Eng. A,* 2003, **360**(1-2), p 18-25
2. J. Lin and W.M. Steen, Design Characteristics and Development of a Nozzle for Coaxial Laser Cladding, *J. Laser Appl.,* 1998, **10**(2), p 55-63
3. K. Van Acker, D. Vanhoyweghen, R. Persoons, and J. Vangrunderbeek, Influence of Tungsten Carbide Particle Size and Distribution on the Wear Resistance of Laser Clad WC/Ni Coatings, *Wear,* 2005, **258,** p 194-202
4. A. Yakovlev, Ph. Bertrand, and I. Smurov, Laser Cladding of Wear Resistant Metal Matrix Composite Coatings, *Thin Solid Films,* 2004, **453-454,** p 133-138
5. D.K. Das, K.S. Prasad, and A.G. Paradkar, Evolution of Microstructure in Laser Surface Alloying of Aluminium with Nickel, *Mater. Sci. Eng. A,* 1994, **174,** p 75-84
6. W.J. Tomlinson and A.S. Bransden, Sliding Wear of Laser Alloyed Coatings on Al-12Si, *J. Mater. Sci. Lett.,* 1994, **13,** p 1086-1088
7. L. Dubourg, H. Pelletier, D. Vaissiere, F. Hlawka, and A. Cornet, Mechanical Characterisation of Laser Surface Alloyed Aluminium-Copper Systems, *Wear,* 2002, **253,** p 1077-1085
8. Y.Y. Qiu, A. Almeida, and R. Vilar, Structure Characterization of a Laser-Processed Al-Mo Alloy, *J. Mater. Sci.,* 1998, **33,** p 2639-2651
9. Y.Y. Qiu, A. Almeida, and R. Vilar, Microstructure of Al 4,3%at Cr Alloy Produced by Laser Surface Alloying, *Scr. Met. Mater.,* 1995, **33**(6), p 863-870
10. Y.T. Pei and J.Th.M. De Hosson, Functionally Graded Materials Produced by Laser Cladding, *Acta Mater.,* 2000, **48,** p 2617-2624
11. L. Dubourg, D. Ursescu, F. Hlawka, and A. Cornet, Laser Cladding of MMC Coatings on Aluminium Substrate: Influence of Composition and Microstructure on Mechanical Properties, *Wear,* 2005, **258**(11-12), p 1745-1754
12. S. Ignat, P. Sallamand, D. Grevey, and M. Lambertin, "Magnesium Alloys Laser Cladding with Side Injection of Aluminium Based Powder," *23rd International Congress on Applications of Lasers and Electro-Optics ICALEO,* Oct 4-7, 2004 (San Francisco, CA), Laser Institute of America
13. L. Dubourg, A. Ott, F. Hlawka, and A. Cornet, Wear Behaviour of Al-Based Composite Coatings Obtained by Laser Cladding and Reinforced with WC, TiC and SiC Particles, *Surface Modification Technologies 18*, SMT 18 (Dijon, France), T.S. Sudarshan, M. Jeandin, and J.J. Stiglich, ASM International, 2004
14. L. Dubourg, B. Des Roches, A. Couture, D. Bouchard, and H.R. Shakeri, "Optimization of Aluminium Laser Welding Using Taguchi and EM Methods," *23rd International Congress on Applications of Lasers and Electro-Optics ICALEO,* Oct 4-7, 2004 (San Francisco, CA), Laser Institute of America
15. L. Dubourg, Experimental Differences between Aluminium Welding of Tee and Lap Joints by a cw/Nd:YAG Laser, *Trends in Welding Research,* May 16-19, 2005 (Pine Mountain, GA)